Q. J. R. Meteorol. Soc. (2005), **131**, pp. 3583–3604 doi: 10.1256/qj.05.105

Operational multivariate ocean data assimilation

By JAMES A. CUMMINGS*
Oceanography Division, Naval Research Laboratory, Monterey, USA

(Received 26 May 2005; revised 21 March 2006)

SUMMARY

A fully three-dimensional, multivariate, optimum-interpolation ocean data assimilation system has been developed that produces simultaneous analyses of temperature, salinity, geopotential and vector velocity. The system is run in real-time, and can be executed as a stand-alone analysis or cycled with an ocean forecast model in a sequential incremental update cycle. Additional capabilities have been built into the system, including flow-dependent background-error correlations and background-error variances that vary in space and evolve from one analysis cycle to the next. The ocean data types assimilated include: remotely sensed sea surface temperature, sea surface height, and sea-ice concentration; plus *in situ* surface and sub-surface observations of temperature, salinity, and currents from a variety of sources, such as ships, buoys, expendable bathythermographs, conductivity–temperature–depth sensors, and profiling floats. An ocean data quality-control system is fully integrated with the multivariate analysis, and includes feedback of forecast fields and prediction errors in the quality control of new observations. The system is operational at the US Navy oceanographic production centres both in global and in regional applications. It is being implemented as the data assimilation component of the Hybrid Coordinate Ocean Model as part of the US contribution to the Global Ocean Data Assimilation Experiment, and in a limited-area ensemble-based forecasting system that will be used in an adaptive sampling, targeted observation application.

KEYWORDS: Background errors Error covariances Forecasting Observation errors Quality control Validation

1. INTRODUCTION

The purpose of this paper is to provide an overview of the ocean data assimilation system in operational use at the US Navy oceanographic production centres: Fleet Numerical Meteorology and Oceanography Center (FNMOC) and the Naval Oceanographic Office (NAVOCEANO). The analysis system is referred to as the Navy Coupled Ocean Data Assimilation (NCODA), and was developed as part of the Naval Research Laboratory coupled modelling projects sponsored by the Office of Naval Research. The analysis can be used in a variety of ways in operations, supporting both global and regional applications. The analysis can be executed in two-dimensional (2D) mode to provide sea surface temperature (SST) and sea ice concentration lower-boundary conditions for the Navy global and regional atmospheric forecast models, or it can be run in 3D mode to provide a stand-alone analysis of ocean temperature, salinity, and geostrophic currents. Alternatively, the analysis can be cycled with an ocean forecast model in a sequential incremental update cycle, providing updated initial conditions for the next ocean model forecast run. The analysis background, or first-guess, fields are generated from a short-term ocean model forecast or from a previous analysis. The analysis computes corrections to the first-guess fields using all of the observations that have become available since the last analysis was made. NCODA has been cycled with a variety of ocean forecast models, including HYCOM (Hybrid Coordinate Ocean Model), NCOM (Navy Coastal Ocean Model), POP (Parallel Ocean Prediction model), and SWAFS (Shallow Water Analysis Forecast System based on the Princeton Ocean Model). The system also supports globally re-locatable, multi-scale analyses on nested, successively higher-resolution grids using a 3:1 nested grid ratio. This nesting strategy is of particular importance in Navy applications where very high resolution is required in a rapid environmental assessment mode of operation.

* Corresponding address: Oceanography Division, Naval Research Laboratory, Monterey, CA 93943, USA.
e-mail: james.cummings@nrlmry.navy.mil

The examples used in the paper are taken from a global 3D analysis running in operational mode at FNMOC, which is described further in section 6. Validation of the analysis system cycling with an ocean forecast model is the subject of a follow-on paper. Here, sections 2 and 3 describe the assimilation method and the techniques used to specify the error covariances. Section 4 lists the ocean observing systems assimilated and outlines the quality control. Sections 5 and 6 summarize the validation and verification features built into the analysis system, and provide a description of the current operational runs and future applications.

2. METHOD

The method used in NCODA is an oceanographic implementation of the multivariate optimum interpolation (MVOI) technique widely used in numerical weather prediction systems. A complete derivation and description of the MVOI method is provided in Daley (1991), with application to atmospheric systems given in Lorenc (1981) and Goerss and Phoebus (1992). The ocean analysis variables are temperature, salinity, geopotential (dynamic height) and velocity. All ocean variables are analysed simultaneously in three dimensions. The horizontal correlations are multivariate in geopotential and velocity, thereby permitting adjustments to the mass fields to be correlated with adjustments to the flow fields. The velocity adjustments (or increments) are in geostrophic balance with the geopotential increments which, in turn, are in hydrostatic agreement with the temperature and salinity increments.

The MVOI problem is formulated as:

$$\mathbf{x}_a = \mathbf{x}_b + \mathbf{P}_b\mathbf{H}^T(\mathbf{H}\mathbf{P}_b\mathbf{H}^T + \mathbf{R})^{-1}\{\mathbf{y} - \mathbf{H}(\mathbf{x}_b)\}, \tag{1}$$

where $\mathbf{x}_a$ is the analysis vector, $\mathbf{x}_b$ is the background vector, $\mathbf{P}_b$ is the background-error covariance matrix, $\mathbf{H}$ is the forward operator, $\mathbf{R}$ is the observation error covariance matrix, and $\mathbf{y}$ is the observation vector. The observation vector contains all of the synoptic temperature, salinity and velocity observations that are within the geographic and time domains of the forecast model grid and update cycle. Observations can be assimilated at their measurement times within the update-cycle time window by comparison against time-dependent background fields using the first-guess at appropriate time (FGAT) method. An advantage of the FGAT method is that it eliminates a component of mean analysis error that occurs when comparing observations and forecasts not valid at the same time.

A forward model is a method of converting a forecast model variable to an observed variable. The MVOI does not explicitly include any forward models, and only analyses observations that are of the same variable as the forecast model. The forward operator used here is spatial interpolation of the forecast model grid to the observation location performed in three dimensions. Thus, $\mathbf{H}\mathbf{P}_b\mathbf{H}^T$ is approximated directly by the background-error covariance between observation locations, and $\mathbf{P}_b\mathbf{H}^T$ directly by the error covariance between observation and grid locations. For the purposes of discussion, the quantity $\{\mathbf{y} - \mathbf{H}(\mathbf{x}_b)\}$ is referred to as the innovation vector, $\{\mathbf{y} - \mathbf{H}(\mathbf{x})\}$ is the residual vector, and $\mathbf{x}_a - \mathbf{x}_b$ is the increment (or correction) vector. The mix of variables with different units in a multivariate analysis requires that the analysis variables be dimensionless. Accordingly, prior to an analysis the innovation vector is normalized by the background error at the observation locations, and after an analysis the increment vector is scaled by the background error at the grid locations.

The solution of (1) is carried out via the overlapping volume approach of Lorenc (1981), with some new capabilities to allow the analysis to interface with any grid.

A total of eight volume solutions are computed for each analysis grid point. The different solutions are weighted by grid point distance from volume centre when forming the final analysis estimate. Volume size is a function of the local correlation length-scale at volume centre, and includes eight correlation length-scales if the number of observations in the volume does not exceed a threshold value (>7200), in which case the volume is subdivided. Note that volume subdivision rarely occurs in practice. The combination of overlapping volumes and a large number of correlation length-scales within a volume, produces analysis increments that are very smooth with no seams along volume edges, and reduces the departure from geostrophy that occurs when interpolating different solutions.

3. Error covariances

Specification of the background- and observation-error covariances in the analysis is very important. The background-error covariances are separated into a background-error variance and a correlation. The correlation is further separated into a horizontal (C_h) and a vertical (C_v) component. All correlations of scalar variables are modelled as second order auto-regressive (SOAR) functions of the form:

$$\begin{aligned} C_h &= (1 + s_h)\exp(-s_h) \\ C_v &= (1 + s_v)\exp(-s_v), \end{aligned} \tag{2}$$

where s_h and s_v are the horizontal and vertical distances between observations or between observations and grid points, normalized by the geometric mean of the horizontal and the vertical correlation length-scales at the two locations. The horizontal correlation length-scales vary with location and depth in the analysis, and the vertical correlation length-scales vary with depth.

(*a*) *Horizontal correlations*

Default horizontal correlation length-scales are specified as the first baroclinic Rossby radius of deformation computed from the historical profile archive (Chelton *et al.* 1998). The Rossby length-scales vary from 10 km at the poles to greater than 200 km in the Tropics. Rossby length-scales can be further modified by a proportionality constant that is set to the ratio of a regionally averaged correlation length-scale computed from an innovation time series using the innovation correlation method (Hollingsworth and Lonnberg 1986; see section 5 below) and the corresponding regionally averaged Rossby length-scales. Proportionality constants computed in this way are on the order of 1.3 to 2.8, with small latitude-dependence. Alternatively, horizontal correlation length-scales can be input directly into the analysis, thereby bypassing the default specifications based on Rossby radius of deformation scales. This option is useful when the horizontal correlation length-scales and other covariance parameters required by the analysis are computed using ensemble methods, as is described in section 6.

Flow-dependence is introduced in the analysis by scaling the horizontal and vertical correlations with a correlation computed from the geopotential height difference between two locations. The flow-dependent correlation (C_f) is computed using a SOAR model, and the total background-error correlation (C_b) is then computed as the product of all three correlation components according to:

$$\begin{aligned} C_f &= (1 + s_f)\exp(-s_f) \\ C_b &= C_h C_v C_f, \end{aligned} \tag{3}$$

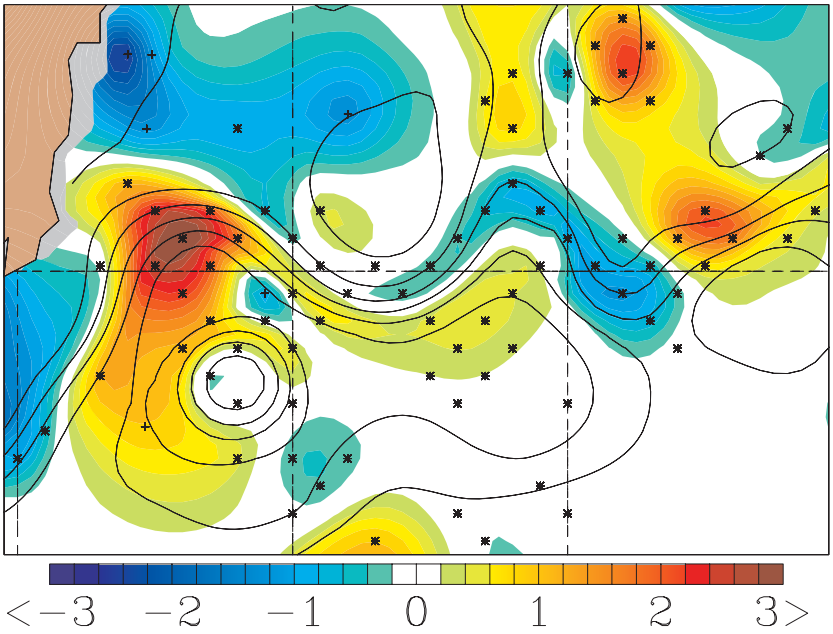

Figure 1. Analysed temperature increments (degC) at 100 m depth in the Kuroshio Extension (colour filled contours). The increment field is extracted from a global three-dimensional multivariate optimum interpolation analysis valid 6 August 2005. Overlay of dynamic height (0/1000 db) contours (contour interval 0.2 dynamic metres) valid 5 August 2005, used to compute the flow-dependent correlations in the analysis (geopotential length-scale $h_s = 0.2$ dynamic metres). Profile observation locations in the analysis are marked using a plus symbol for Argo floats and conductivity temperature depth casts, and asterisks for Modular Ocean Data Assimilation System synthetics.

where s_f is the geopotential height difference at two locations normalized by a specified geopotential length-scale (h_s), and C_h and C_v are as described above. A small (large) value of h_s will produce strong (weak) flow-dependence in the analysis increments. The flow-dependent correlations tend to spread the innovations along rather than across geopotential contours. This is a desirable outcome, since error correlations across an ocean front are expected to be characteristically smaller than error correlations along the front. An example of this calculation is shown in Fig. 1, which shows the flow-dependent analysis increments from a global 3D MVOI analysis in the vicinity of the Kuroshio Extension western boundary current front east of Japan, and the geopotential background field valid the previous day that was used to compute the flow-dependent correlations. The temperature increments are clearly constrained by the meanders of the Kuroshio front as it leaves the coast, and a strong cold-core eddy south of the front. A potential drawback to this method is that the flow-dependent correlations are computed directly from the forecast model height fields, thus they depend strongly on the accuracy of the model forecast. This is equivalent to an assumption of a perfect model, and may not prove to be very useful in practice if the forecast model fields are inaccurate. Accordingly, flow-dependence can be switched off, or h_s can be set to a relatively large value, to prevent, or minimize, a model forecast with systematic error from adversely affecting the analysis.

(*b*) *Vertical correlations*

A variety of options are available in the analysis to specify the vertical correlation length-scales. Vertical correlation length-scales can: (i) be constant (or zero), (ii) monotonically increase or decrease with depth, or (iii) vary with background density vertical gradients. In the latter option, a change in density stability criterion is used to define a well-mixed layer. The change in density criterion is then scaled by the background vertical density gradient according to:

$$h_{\mathrm{v}} = \rho_{\mathrm{s}}/(\partial\rho/\partial z), \tag{4}$$

where h_{v} is the vertical correlation length-scale, ρ_{s} is the change in density criterion, and $\partial\rho/\partial z$ is the vertical density gradient. The resulting vertical correlation length-scales vary with depth and are large (small) when the water column stratification is weak (strong). The vertical correlations are computed each update cycle from the background density fields. This process allows the vertical-scales to evolve from one analysis cycle to the next to capture changes in mixed layer and thermocline depths.

(*c*) *Multivariate correlations*

The horizontal correlation functions described above are used in the analysis of temperature, salinity and geopotential, and all of these variables are assumed to have the same background-error correlations. The formulation of the multivariate background-error correlations, however, is derived from the first and second derivatives of the SOAR model function. This form requires the calculation of the angles between the two locations and the specification of a parameter ν, which measures the divergence permitted in the velocity correlations, and a parameter μ, which specifies the strength of the geostrophic coupling of the velocity/geopotential correlations. Typically, ν is set to a constant small value ($\nu = 0.05$) that does not vary with location. This setting will produce velocity increments that are weakly divergent, and assumes that the divergence is not correlated with changes in the mass field. Parameter μ, however, does vary from 0 to 1 with location. It is scaled to zero within 2° of latitude from the equator where the f-plane geostrophic equation is singular, and in shallow water <50 m deep where friction rather than pressure gradient forces controls ocean flow. As mentioned previously, a full derivation of the multivariate horizontal correlations is provided in Daley (1991). Using the derivatives of the geopotential SOAR correlation model and converting from natural to rectangular coordinates, the correlation functions of the possible combinations of geopotential and velocity are shown in Fig. 2. There are nine possible combinations, but for clarity only one form of the cross-correlations between geopotential and the velocity components is shown.

(*d*) *Background-error variances*

Background-error variances are poorly known in the ocean and are likely to be strongly dependent on model resolution and other factors, such as atmospheric model forcing errors and ocean model parametrization errors. In the analysis, the background-error variances (e_{b}^2) vary with location, depth, and analysis variable, and are computed prior to an analysis from a time history of the analysed increment fields according to:

$$\begin{aligned} \beta &= \exp(-\tau/\tau_{\mathrm{c}})^2 \\ e_{\mathrm{b}}^2 &= \beta \cdot \left(\sum_{k=1}^{n} \mathbf{w}_k (\mathbf{x}_{\mathrm{a}} - \mathbf{x}_{\mathrm{b}})_k^2 + \mathbf{w}_{n+1} \langle (\mathbf{x}_{\mathrm{a}} - \mathbf{x}_{\mathrm{b}})^2 \rangle \right) + (1 - \beta) \cdot \sigma_{\mathrm{b}}^2, \end{aligned} \tag{5}$$

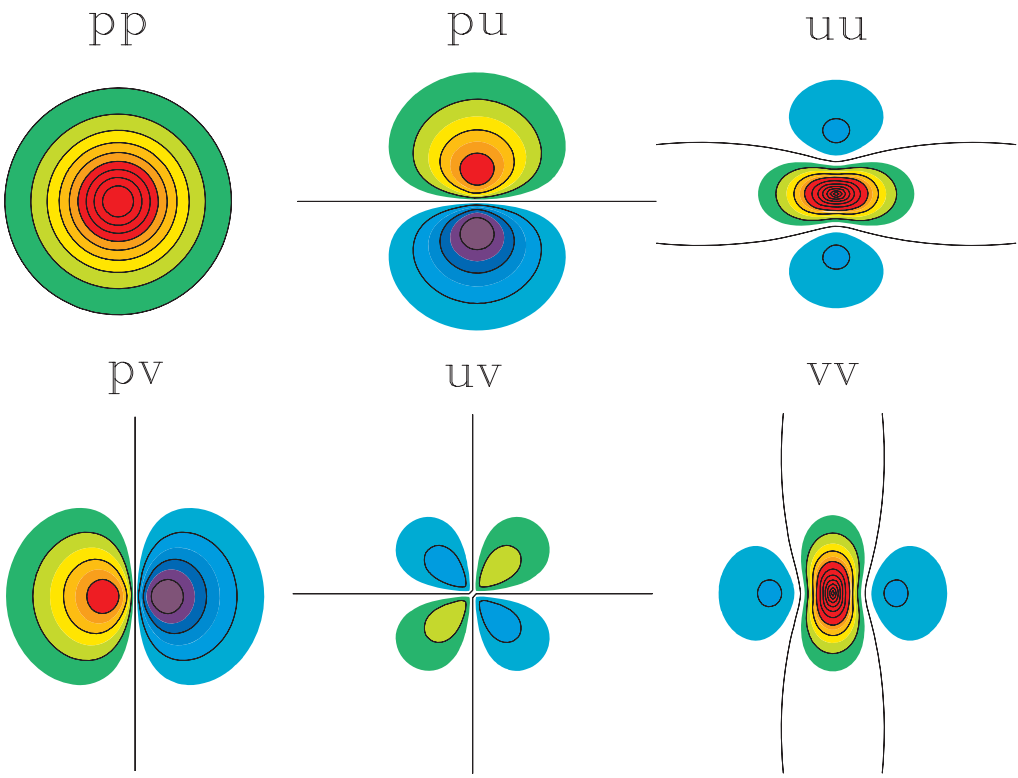

Figure 2. Auto- and cross-correlations of horizontal multivariate correlation functions for geopotential (p), **u** vector component of ocean current velocity (u), and **v** vector velocity (v). Warm (cool) colours indicate positive (negative) correlations. The multivariate correlation functions have been computed with the geostrophic coupling parameter set to 1.0 and the divergence parameter set to 0.1 (see text for details).

where c refers to a fixed climate time-scale, $\mathbf{x}_a - \mathbf{x}_b$ is the increment vector (indices indicating grid location and depth are omitted for clarity), $\mathbf{w}$ is the weight vector, $\langle \ldots \rangle$ indicates a long-term mean increment vector over all update cycles into the past older than the number of recent update cycles n; k is the update cycle index, τ is the age of the data ($\tau > 0$), τ_c is an integral time-scale, σ_b^2 is the expected variance of the analysis variable, and β is a factor that combines the error contributions from the increments and expectations based on age of the data on the grid. The first and second terms on the right-hand side of (5) compute the background error from the analysis increment fields, with recent increments more heavily weighted than errors accumulated over many update cycles. Elements of the increment vector must exceed a minimum threshold value $|\mathbf{x}_a - \mathbf{x}_b| > \delta$ in order to be used in the summations, where the magnitude of δ depends on the analysis variable. Weight vector, $\mathbf{w}_k$, is computed using a geometric series, $\mathbf{w}_k = (1 - \phi)^{k-1}$, where ϕ is a tunable constant between 0 and 1 (typically set to 0.2), and normalized such that the weighted averages are unbiased. The third term on the right-hand side of (5) allows the background-error variances to increase with time in the long-term absence of observations until the errors asymptote at the limit of the expected variance (σ_b^2), specified as either climate variability or model error. If available, model error is computed from a multi-year time series of differences between free running model states at the analysis update cycle time interval.

The relaxation to an expected error variance is needed because not all analysis grid locations are corrected in every update cycle, due to sampling limitations of the ocean observing systems. In order to distinguish between a zero increment indicating a perfect model forecast or simply no data, the age of the data on the grid (τ) is computed. Age of the data is defined as the number of hours since a grid location has been influenced by an observation. It can be negative, indicating the influence of observations younger than the analysis time. Observation age innovations are computed as the difference between the observation time and the valid time of the analysis, and assimilated as an uncorrelated scalar using the same error correlations as the mass variables. The background age field is increased by the number of hours in the update cycle at the beginning of an analysis and can only be reduced by the assimilation of synoptic data. Time-scales (τ_c) specified independently for each analysis variable are used to normalize age of the data on the grid. The time-scales range from $\sim$10 days for surface- and mixed-layer variables to $\sim$30 days for variables at depth. Evaluation of time-scales computed using a relationship between the modified Rossby length-scales (d) and current speed (s), given by $\tau_c = d/s$, is underway. Here, time-scales vary with location and depth, and range from a few days near the surface in high speed, western boundary current regions, to $\sim$7 years in the deep ocean where current speeds are slow.

In practice, the background-error variances evolve to a quasi-steady state over time. Figure 3 shows examples of the background error and age of the data on the grid for SST, altimeter sea surface height anomaly (SSHA), and temperature at 400 m depth, from a global 3D MVOI analysis cycled from 20 June to 1 November 2005 using a 24-hour update cycle. The number of increment fields into the past and time-scales used in the summations are 10 days for SST, 20 days for SSHA, and 30 days for temperature at depth. SST data age shows that the SST field is well constrained by observations, with the result that SST background errors are primarily a function of the analysis increments. SSHA data age shows the characteristic diamond-shaped data void areas between altimeter satellite tracks, and data age at 400 m shows numerous areas that have not been observed for 4 weeks or more, such as the south-east Pacific and eastern Atlantic. SSHA and temperature background errors at depth are, therefore, a mix of analysis increment errors and climate errors, due to the lack of observations in some locations for extended time periods. As expected from an analysis cycling on itself, the background errors tend to reflect variability associated with western boundary currents. However, the pattern and the magnitude of the background errors are expected to be very different when the analysis is cycled with an ocean forecast model as a first-guess. Ocean mesoscale variability will be increased by contributions from atmospheric forcing and ocean model errors, and reduced by ocean model forecast skill.

The adaptive scheme implemented here is designed to provide background errors that: (i) are appropriate for the time interval at which data are inserted into the model, (ii) are coherent with the variance of the innovation time series, (iii) reflect the variable skill of the different ocean forecast models that are used with the analysis system, (iv) adjust quickly to new ocean areas when the analysis is re-located in a rapid environmental assessment mode of operation, and (v) can be computed when the analysis is cycled on itself or with a forecast model. One difficulty with using analysis increments to compute background-error variances is that the increments contain a mixture of forecast and analysis error. Analysis errors result from the fact that the statistical parameters used in the analysis represent expected values, and are unlikely to be correct at all places and at all times. While the analysed increment approach may not represent all aspects of the background error, the method does provide a reasonable measure of the spatial structure of the background errors. Inaccuracies in the magnitudes

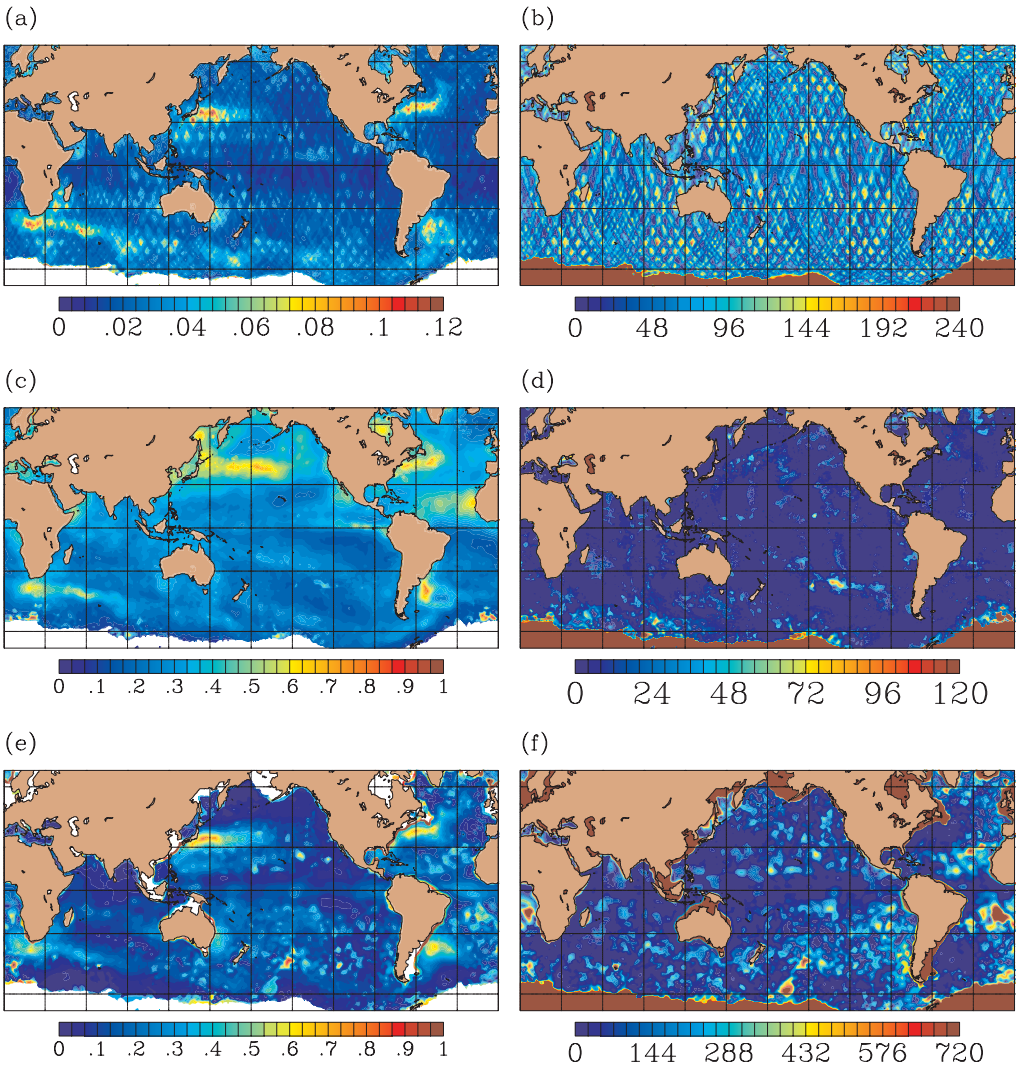

Figure 3. Background-error standard deviations and age of the data on the grid from a global three-dimensional multivariate optimum interpolation analysis valid 1 November 2005: (a) sea surface height anomaly (SSHA) background errors (m); (b) SSHA data age; (c) sea surface temperature (SST) background errors (degC); (d) SST data age; (e) temperature errors at 400 m (degC); (f) age of the data at 400 m. Ages are given in hours. White areas represent ice covered seas or grid locations shallower than 400 m. Note differences in the colour scales between panels.

of the background-error variances are adjusted with the $J_{\min}$ diagnostic described in section 5.

(*e*) *Observation-error variances*

The observation errors and the background errors are assumed to be uncorrelated, and errors associated with observations made at different locations and at different times are also assumed to be uncorrelated. As a result of these assumptions, the observation-error covariance matrix $\mathbf{R}$ is set equal to $1 + E_0^2$ along the diagonal and zero elsewhere, where E_0^2 represents observation-error variances normalized by the background-error

variances interpolated to the observation location. (Recall from section 2 that the innovation vector in (1) is normalized by e_b^2). This noise-to-signal ratio will vary from one update cycle to the next, since the background errors and the components of some of the observation errors change with time and location in the analysis.

Observation errors are computed as the sum of a measurement error (e_m^2) and a representation error (e_r^2). Measurement-error variances are specified as input parameters in the analysis with one exception that is described below. Measurement errors reflect the accuracy of the instruments and the ambient conditions in which they operate. These sources of error are fairly well known in the ocean for many observing systems, although the magnitudes of the measurement errors can change in time due to calibration drift of the instruments and other factors. Some observing system measurement errors are now included in the real-time data stream by the data providers. For example, satellite SST retrieval errors are routinely computed using a sliding time window of space–time collocations of drifting buoy measurements of SST and satellite SST retrievals. These error estimates vary with the satellite platform, retrieval algorithm and time. Data sources that have fixed specifications of measurement error are listed in Table 1.

Representation errors, however, are a function of the resolutions of the model and of the observing network, and are much more difficult to quantify. A satellite retrieval representation error is computed when the resolution of the retrieval (r_s) exceeds the resolution of the grid (r_g) according to:

$$e_{\text{r-sat}} = \nabla_f \cdot (r_s / r_g), \tag{6}$$

where $e_{\text{r-sat}}$ is the representation error of the satellite retrievals, ∇_f is the gradient of the background field at the retrieval location, and $r_s > r_g$. Analysis grid resolutions commonly used in operations are ~9–18 km (section 6), which results in an increase of the representation errors of microwave (25 km) and Geostationary Operational Environmental Satellite (GOES) SST (12 km), and Special Sensor Microwave/Imager (SSM/I) sea ice (25 km) retrievals in high-gradient regions. Other satellite data with smaller footprint sizes, such as altimeter SSHA (7 km) and infrared satellite SST (8 km), are not affected. Representation error of temperature and salinity profile observations is assumed to be dependent on the mesoscale signal and an uncertainty associated with internal wave activity. Using climate variability as a proxy for the mesoscale signal, and the observed vertical gradient as a proxy for the aliasing error associated with internal waves, profile temperature ($e_{\text{r-tmp}}$) and salinity ($e_{\text{r-sal}}$) representation errors are computed by:

$$\begin{aligned} e_{\text{r-tmp}} &= \kappa_T \sigma_T + \lambda_T (\mathrm{d}T/\mathrm{d}z) \\ e_{\text{r-sal}} &= \kappa_S \sigma_S + \lambda_S (\mathrm{d}S/\mathrm{d}z), \end{aligned} \tag{7}$$

where σ_T and σ_S are the climate temperature and salinity standard deviations at the observation location and sampling time, and $\mathrm{d}T/\mathrm{d}z$ and $\mathrm{d}S/\mathrm{d}z$ are the observed temperature and salinity vertical gradients. The constants $\kappa_{T,S}$ and $\lambda_{T,S}$ are determined empirically; they are currently set to 0.01 and 0.3, respectively, for both temperature and salinity. Since observing system representation error is so poorly known, it is implemented as a tunable parameter in the analysis. The $J_{\min}$ diagnostic (described in section 5) is used to determine changes needed in the magnitude of the representation error.

The exception to the off-line specification of the observation-error variances is that of the geopotential observations. Geopotential is computed during an analysis from the temperature and salinity observations, by integrating the specific-volume anomaly (Fofonoff and Millard 1983) from a level of no motion to the surface. The errors, e_α,

TABLE 1. GLOBAL OPERATIONAL OCEAN OBSERVATION DATA SOURCES

Data source	Specifications	Estimated number of daily observations	Measurement-error standard deviations
AVHRR GAC[1] Infrared Satellite SST	8 km day, night, relaxed day retrievals NOAA-16, 17, 18	1 200 000	variable
AVHRR LAC[2] Infrared Satellite SST	2 km day, night retrievals NOAA-16, 17, 18	4 000 000	variable
GOES Infrared Satellite SST	12 km day, night retrievals GOES-10, 12	5 000 000	variable
Microwave Satellite SST	AMSR-E 25 km retrievals	5 000 000	variable
Thermosalinograph	*in situ* SST, SSS[3]	1 800	1.1 degC, 0.5 PSU
Sea surface height anomaly	Satellite altimeters (Jason, GFO[4] and Envisat)	150 000	0.03, 0.08, 0.08 m
	T and S profiles	300	0.01 m
Sea ice concentration	SSM/I 25 km retrievals DMSP[5] F13, F14, F15	1 200 000	5%
Ship SST	Engine room intake	4 000	1.3 degC
	Hull contact sensor	800	0.6 degC
	Bucket temperature	200	1.2 degC
Buoy SST	Fixed	6 000	0.05 degC
	Drifting	32 000	0.12 degC
CMAN[6] Stations	*in situ* SST	120	1.1 degC
XBT	Temperature profiles	100	0.12 degC
Argo Floats	Temperature and Salinity profiles	200	0.002 degC 0.01 PSU
CTD[7] Stations (TESACs[8])	Temperature and Salinity profiles	50	0.002 degC 0.01 PSU
Drifting Buoy	Temperature profiles	700	0.12 degC
Fixed Buoy	Temperature and Salinity profiles	1 000	0.003 degC 0.02 PSU

[1] Global area coverage.
[2] Local area coverage.
[3] Sea surface salinity.
[4] Geosat Follow On.
[5] Defense Meteorological Satellite Program (USA).
[6] Coastal Marine Automated Network.
[7] Conductivity Temperature Depth.
[8] Temperature, salinity and currents; a type of WMO message form.
See text for other details.

in specific-volume anomaly, α are computed from the errors, e_θ and e_S, of the potential temperature θ, and salinity, S, observations, using the partial derivatives of the equation of state with respect to θ and S according to:

$$e_\alpha = (\partial\alpha/\partial\theta)e_\theta + (\partial\alpha/\partial S)e_S. \tag{8}$$

The specific-volume anomaly errors are then integrated through the water column from the user-defined level of no motion to the surface in the same way as the geopotential itself is integrated. Geopotential errors at and below the level of no motion are set to a small value.

4. Ocean observations

The analysis makes full use of all sources of operational ocean observations. The ocean observing systems currently assimilated are listed in Table 1, along with typical global data counts per day for the different observing system categories. New data sources are continually being added to the analysis, such as surface velocity observations from high-frequency coastal radar installations. In addition to satellite altimeters, SSHA observations computed from *in situ* profiles of temperature and salinity are used as a source of data in the SSHA analysis. The *in situ* SSHA observations constrain the extrapolation of the satellite altimeter sea surface height (SSH) data by the analysis into the diamond shaped areas that otherwise are not observed by nadir sampling altimeters. This feature is important when the satellite altimeter data assimilated are from a short repeat cycle mission ($\sim$10 days) with large distances ($\sim$300 km) between adjacent tracks.

(*a*) *Quality control*

All ocean observations are subject to data quality-control (QC) procedures prior to assimilation. The need for QC is fundamental to a data assimilation system. Accepting erroneous data can cause an incorrect analysis, while rejecting extreme but valid data can miss important events. It is likely that decisions made at the QC step affect the success or failure of the entire analysis/forecast system. A complex QC process is used in which an observation is not rejected as soon as it fails an individual QC test. Rather, each observation is subjected to a series of tests, with the final QC decision based on consideration of all of the QC test results. The real-time QC system described in Cummings (2006) is summarized here.

A sequence of gross-error data checks are performed first, which include a land–sea boundary test, valid-value range tests, and a location (speed) test for platforms that report unique call signs. Next, a series of instrumentation error checks are performed on expendable bathythermographs and profiling floats; sensor drift in fixed and drifting buoys is checked, and a test for aerosol contamination is performed on satellite SST retrievals. Cross validation checks are also performed to ensure the consistency of observations within and between analysis variables. In the within-variable consistency check, an optimum interpolation (OI) analysis is performed at each of the newly received observation locations and sampling times based on nearby valid data, excluding the datum being checked, using innovations computed from climatology. The uncertainty of the analysed value is computed from the OI reduction of climate error due to the introduction of nearby observations. In the absence of any nearby data, the consistency check simply returns climatology and climate variability as the analysis estimates. The cross validation analysed value and its uncertainty are used in the background-field check described below. The cross validation of profile observations works well in practice because of the continuing development of the Argo profiling float array (Argo Science Team 1998) and the large number of high quality, deep profiles that are available to use in the procedure. Cross validation consistency checks are also very useful in the QC of altimeter SSHA observations, since those data tend to be spuriously rejected along sequential segments of altimeter tracks due to phase errors in the model background fields. Examples of cross validation consistency checks between analysis variables include: SST and sea ice concentration to check for impossible ice conditions; and wind speed and daytime satellite SST retrievals to check for biases due to diurnal warming skin temperature effects. These procedures produce integer-valued QC flags of varying levels of severity, ranging from information-only (<100), cautionary (>100) and fatal (>1000).

The most important QC procedures are the background-field checks, which include climatology, and global and regional analyses or short-term forecasts. The background and background-error fields closest in time to the observation sampling time are interpolated to the observation location. The probability of an erroneous value is calculated from the difference between observed and background values, assuming an unbiased normal distribution with appropriate climate-, analysis- or prediction-error standard deviations. Histograms and formal statistical tests show that the innovations are normally distributed, although climate innovations tend to have very long tails. In addition to the level-by-level field checks described above, observed profiles are compared to profiles extracted from the various background fields and cross validation profiles using a profile-shape QC procedure. This procedure computes an integrated probability of random error that takes into account level-thicknesses when comparing observed and predicted values, and has the advantage of taking an overview of the entire profile. The background-field and shape-error probabilities are used in combination with the QC flags in a decision-making algorithm when selecting observations for the assimilation. (Quality controlled ocean observations used in the FNMOC MVOI analyses are available on the US GODAE data server http://www.usgodae.org/ in near real-time.)

Within the analysis itself a final QC procedure is performed to remove observations that have passed the error checks described above but that may still be unacceptable to the analysis background. This procedure is referred to as the innovation-error check and is done in the following way. Given the diagonal of $\mathbf{HP}_\mathrm{b}\mathbf{H}^\mathrm{T} + \mathbf{R}$ and the $\mathbf{y} - \mathbf{H}(\mathbf{x}_\mathrm{b})$ innovation vector, compute the normalized innovations as $\mathbf{d} = \mathrm{diag}(\mathbf{HP}_\mathrm{b}\mathbf{H}^\mathrm{T} + \mathbf{R})^{-1/2}\{\mathbf{y} - \mathbf{H}(\mathbf{x}_\mathrm{b})\}$. The elements of the normalized innovation vector over many realizations should be a normal distribution with a standard deviation equal to one if the background- and the observation-error covariances $\mathbf{P}_\mathrm{b}$ and $\mathbf{R}$ have been properly specified. Assuming this to be the case, tolerance limits (T_L) are defined to remove unacceptable observations. The tolerance limits are equivalent to the number of acceptable standard deviations of the innovation from the analysis background. Since $\mathbf{P}_\mathrm{b}$ and $\mathbf{R}$ are never perfectly known, it is best to use a higher tolerance value rather than a lower one in this procedure. The test statistic is 'reject the observation if $\mathrm{d} > T_\mathrm{L}$', where $T_\mathrm{L} = 4$ is specified.

(*b*) *Pre-processing of ocean observations*

Several pre-processing functions are performed on the quality-controlled ocean observation datasets prior to assimilation. All surface data types are reduced in number by the formation of 'super-observations'. Super-observations are innovations averaged into bins that are dependent on the grid resolution and the observation data type. Thinning of observations is a necessary step in the analysis in order to remove redundancies in the data and minimize horizontal correlations among observations. The super-observation algorithm used to thin data in the analysis is adaptive. As the model grid resolution increases, the actual number of innovations averaged into a super-observation decreases until, eventually, the original data are directly assimilated. This feature is very useful in a nested analysis run, where the nested grids telescope down to the desired forecast model grid resolution.

SST observations are stratified further by water mass in western boundary current regions. The water mass classification is based on Bayes rule, given here in density form:

$$\begin{aligned} p(i \mid x) &= p(x \mid i)p(i)/p(x) \\ p(x \mid i) &= N(x \mid \mu_i, \sigma_i), \end{aligned} \tag{9}$$

where $p(i \mid x)$ is the a posteriori probability of water mass i, given temperature x, $p(i)$ is the a priori probability of occurrence of the ith water mass, and $p(x \mid i)$ is the conditional probability of temperature x given water mass i, which is a normal probability distribution function with parameters (μ_i, σ_i). The Bayesian water mass classification statistics are computed off-line from analyses of temperature frequency distributions using monthly datasets of Advanced Very High Resolution Radiometer (AVHRR) SST retrievals. The frequency distribution analysis computes the best fit of a mixture of normal probability distribution functions that describe the observed, polymodal frequency distribution. The number of modes (water masses), and the maximum likelihood estimates of the means (μ_i) and standard deviations (σ_i) of the composite normal distributions in the mixture, provide the necessary classification statistics. Figure 4 shows the SST frequency distribution for the month of July in the Brazil–Malvinas confluence area with an overlay of the best-fit mixture of normal probability distributions. The water mass classification decision boundaries are the local minimums of the overlapping normal probability distributions. Figure 4 also shows the geographic distribution of water mass classified Advanced Microwave Scanning Radiometer (AMSR)-E microwave SST observations for 16–17 July 2005. This independent, synoptic SST dataset clearly shows the boundaries of the narrow ocean fronts and associated mesoscale eddies. The water mass classification of SST observations prevents the averaging of dissimilar observations across ocean fronts and eddies during the formation of the super-observations. This process helps to maintain horizontal SST gradients in the analysis. In addition to the Brazil–Malivinas confluence, water mass classification statistics have also been computed for the Agulhas Current, Gulf Stream, Kursohio Extension, Sea of Japan, and East Australian Current regions.

Pre-processing options on the profile data include: (i) specification of selection criteria to ensure adequate sampling in the vertical, (ii) vertical extension of the profiles from the last observed depth to the bottom using the first-guess background field, and (iii) assimilation of profile observations at observed levels or after vertical interpolation to model levels.

(*c*) *Altimeter sea surface height assimilation*

From Table 1, it is apparent that most ocean observations are remotely sensed and measure ocean variables only at the surface. The lack of synoptic real-time data at depth, places severe limitations on the ability of the data assimilation system to resolve and maintain an adequate representation of the ocean mesoscale. Sub-surface properties in the ocean, therefore, must be inferred from surface-only observations. The most important observing system for this purpose is satellite altimetry, which provides measures of the time varying change in SSH in the form of anomalies from an 8-year repeat track mean. Changes in SSH are strongly correlated with changes in the depth of the thermocline in the ocean, and the ocean dynamics generating SSH changes are the mesoscale eddies and meandering ocean fronts. Two alternative methods can be used in the analysis to assimilate satellite altimeter observations of SSHA. In neither method is the altimeter data directly used to change the background fields. Rather, altimeter-derived synthetic profile observations are computed, and combined in the analysis with *in situ* observations and the model background, which requires specifying observation errors of the synthetic profiles.

One approach is the assimilation of synthetic temperature profiles computed using the Modular Ocean Data Assimilation System (MODAS) database. MODAS models the time-averaged co-variability of SSH and temperature at depth at a fixed location (Fox *et al.* 2002). Regression coefficients derived from the historical profile archive have been

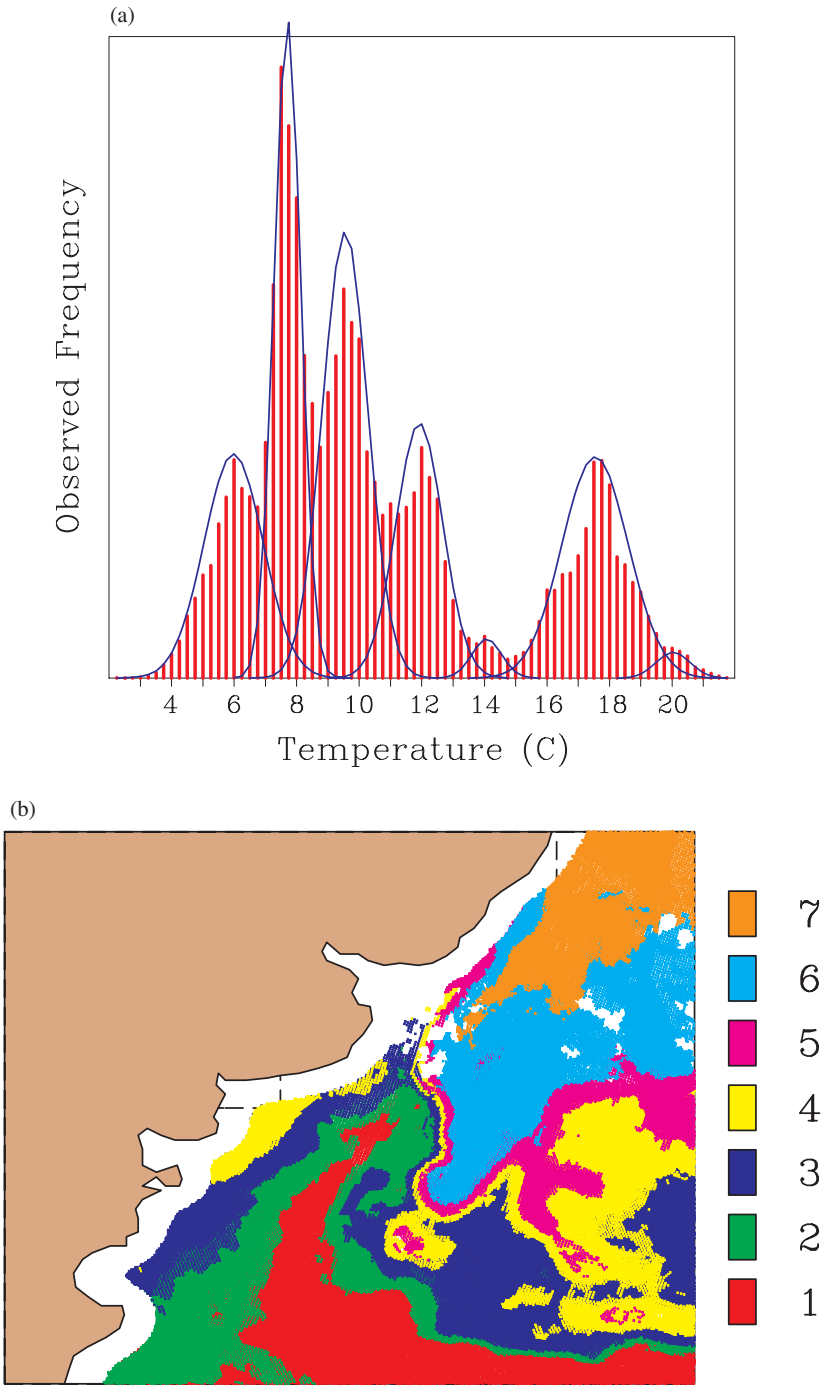

Figure 4. (a) Observed (histogram) and fitted (solid curve) frequency distribution of AVHRR global area coverage satellite sea surface temperature (SST) retrievals in the Brazil–Malvinas confluence region for the month of July. Frequency distribution binning interval is 0.25 degC. (b) Geographic distribution of water mass classified AMSR-E microwave satellite SST retrievals for 16–17 July 2005. Water mass classification numbers are defined from cold to warm temperature modes in the fitted frequency distribution. The binning interval is 0.25 degC and the frequencies plotted have been normalized to range from 0 to 1 for display purposes.

computed that relate steric height anomalies to climate temperature anomalies at depth. The error variances of the MODAS synthetic profiles in the analysis depend upon the accuracy of the SSH predictor field and upon the magnitude of the residual errors of the regressions relating steric height and temperature at depth. MODAS residual errors vary with location, depth and time of year, and are generally small in western boundary current regimes where steric height anomalies are highly correlated with changes in the depth of the thermocline. MODAS has marginal skill in other areas of the world's oceans due to: (i) sampling limitations of the historical profile data, (ii) non-steric signals in the altimeter data, and (iii) weak correlations between steric height and temperature at depth due to other factors, such as the influence of salinity on steric height at high latitudes and in eastern boundary regions. Salinity profiles are computed from the synthetic MODAS temperature profiles in a subsequent, separate step as described in subsection 4(d). The MODAS synthetic temperature and derived salinity profile method is primarily used when the analysis system is cycling on itself.

A second and alternative approach is the direct assimilation of observed SSH changes using a modified form of the method developed by Cooper and Haines (1996). In this approach, the model forecast density field is adjusted to correct errors between the model height field and the height field measured by the altimeter. The adjustments are computed by:

$$\Delta p_{\mathrm{s}} + g \int_{z_{\mathrm{b}}}^{z_{\mathrm{t}}} \Delta \rho_z \, \mathrm{d}z = \Delta p_{\mathrm{b}}, \tag{10}$$

where Δp_{s} is the surface pressure change measured by the difference between the model background and the satellite altimeter observation, $\Delta \rho_z$ is the change in density at level z, g is the gravitational constant, and Δp_{b} is the bottom pressure change. The depth range of the density corrections is constrained to be between the mixed layer (z_t) and a level of no motion (z_{b}) where Δp_{b} is assumed to be zero. Output of the integration is in the form of innovations of temperature and salinity from the background field. The observation-error variances of the temperature and salinity innovations are computed as the sum of the respective background-error variance plus the residual error from the iterative fit of the density adjustments to the observed change in SSH. An advantage of this direct method over the MODAS method is that it relies on model dynamics for a priori information rather than statistics fixed at the start of the assimilation. Furthermore, the method computes adjustments to the model temperature and salinity profiles simultaneously. As a result, it does not introduce spurious water masses into the model. A disadvantage is that the direct method cannot explicitly correct for errors in the stratification or long-term drift of the water mass characteristics in the model. Also there are difficulties applying the direct method in weakly stratified conditions (Fox *et al.* 2000) which occur primarily at high latitudes. Accordingly, altimeter SSHAs are scaled to zero at latitudes greater than 65°. The direct method is only used when the analysis is cycled with an ocean forecast model.

While having the potential of adding important information in data-sparse areas, the number of altimeter-derived synthetic observations computed can greatly exceed and overwhelm the *in situ* observations in the analysis. Accordingly, the synthetic observations are thinned prior to the analysis in three steps. In the first step, it is assumed that directly observed temperature and salinity profiles are a more reliable source of subsurface information wherever such observations exist. Altimeter-derived subsurface profiles, therefore, are not generated in the surrounding area of an *in situ* profile observation defined by the local correlation length-scale. In the second step, the analysed incremental change in SSH measured by the altimeter must exceed a

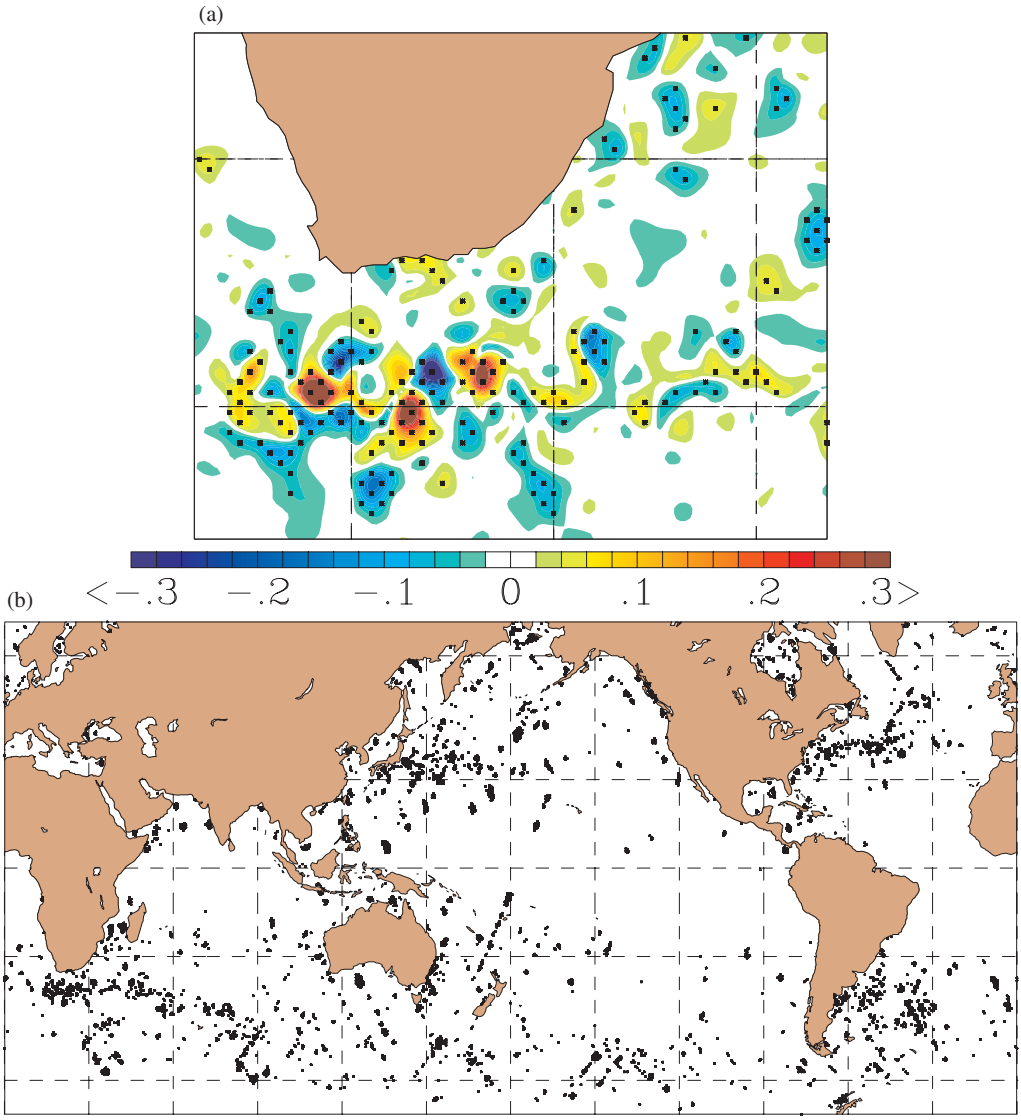

Figure 5. Synthetic profile sampling pattern for a global three-dimensional multivariate optimum interpolation analysis valid 21 October 2005: (a) altimeter sea surface height anomaly (SSHA) analysis increments (colour filled contours) with synthetic profile locations (dots) in the Agulhas current subdomain of the global grid where the absolute value of the SSHA increment exceeds 4 cm; (b) global locations of synthetic profiles generated from SSHA increments. A total of 3862 synthetic profile locations were sampled, which created 99 210 synthetic temperature–salinity depth observations in the analysis.

threshold value, defined as the noise level of the satellite altimeters, to trigger the generation of a synthetic observation. Finally, in the third step, local correlation length-scales are used to control the density of the synthetic profiles within the contours of SSH change that exceed the prescribed noise-level threshold. An example of the synthetic profile sampling pattern generated in a global MVOI analysis is shown in Fig. 5. Figure 5(a) shows the synthetic profile locations in relation to the analysed SSHA

increments in the vicinity of the Agulhas current, using a noise-level threshold value of 4 cm; Fig. 5(b) shows the global distribution of altimeter-derived synthetic profiles generated primarily in western boundary current regions and the Antarctic circumpolar current, where the daily change in SSHA is large due to mesoscale variability.

(*d*) *Salinity observations*

In the multivariate analysis, observed temperatures must have a companion salinity observation in the computation of the geopotential observations. Salinity is routinely measured by some observing systems, such as Argo floats and shipboard conductivity–temperature–depth (CTD) profiles, but other observing systems measure only temperature. For these observing systems, salinity is estimated from the observed temperature using temperature–salinity regression relationships derived from the historical profile archive and stored in the MODAS database. The observation-error variance of the derived salinity values is estimated from the residuals of the MODAS regressions, which vary in both space and time. MODAS-derived salinities have good skill at depths where the temperature–salinity relationship is well defined and the historical profile archive is adequate, as shown by independent verification against Argo and shipboard CTD profiles. Near the surface this relationship breaks down, and the derived salinities tend to reflect the climate mean that is used as the basis function in the regressions. However, the near-surface regression residuals, and thus the observation errors, are also large, with the result that MODAS-derived salinity observations near the surface carry little weight in the analysis.

5. Validation and verification

Residual vectors $\{\mathbf{y} - \mathbf{H}(\mathbf{x}_a)\}$ are routinely computed for each analysis variable. The residuals and the innovations for all observations assimilated are saved at the end of each update cycle in an innovation-vector file. When cycling with an ocean forecast model the analysis system also saves forecast field values at the observation locations for all forecast periods that are multiples of the analysis update cycle time interval. These observation innovation- and forecast-vector files allow rapid assessment of the impact of the assimilation on the skill of the forecast, which is a useful diagnostic tool for determining the performance of the analysis. A time history of the innovations and the residuals is the basic information needed to compute a posteriori refinements to the statistical parameters required in the MVOI. Statistical analysis of the innovations is the most common, and the most accurate, technique for estimating observation- and forecast-error covariances, and the method has been successfully applied in practice (e.g. Hollingsworth and Lonnberg 1986). Examination of the residual vectors is also very useful in assessing the fit of the analysis to specific observations or observing systems. A spatial autocorrelation analysis of the residuals is used to determine if the analysis has extracted all of the information in the observing system. Any spatial correlation remaining at spatial lags greater than zero represents information that has not been extracted by the analysis and indicates an inefficient analysis. Figure 6 shows the results of a binned average, spatial autocorrelation analysis of the innovations and residuals of drifting buoy SST observations for April 2005 in the global 3D MVOI analysis. The spatial averaging bins are determined by the resolution of the analysis grid. A SOAR model is a good fit to the innovation autocorrelations, and the analysis residuals are uncorrelated at all spatial lags greater than one. However, the positive correlation in the first spatial bin of the residual autocorrelation indicates that the analysis does not fit the data to within the specified observational error limits and is suboptimal

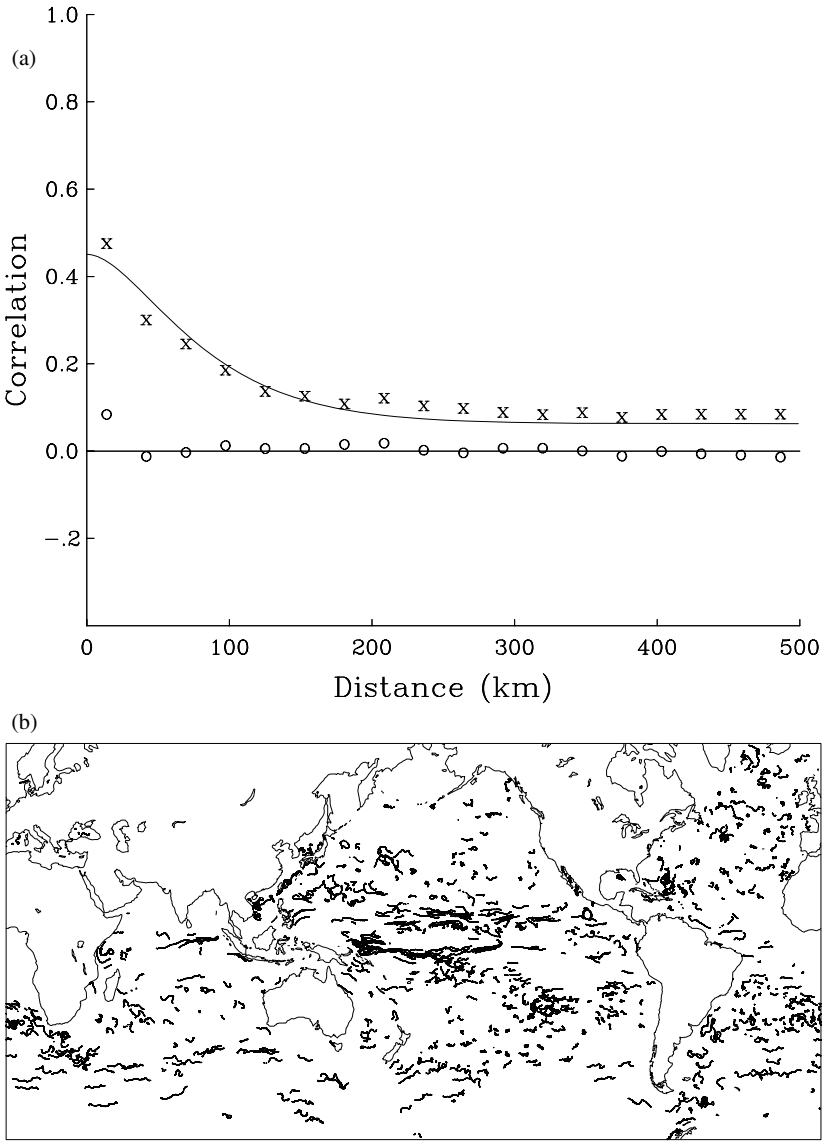

Figure 6. (a) Spatial autocorrelation analysis of drifting-buoy sea surface temperature (SST) innovations and residuals from global three-dimensional multivariate optimum interpolation analyses for April 2005. Innovation autocorrelations are marked **X** and residual autocorrelations are marked **O**. The solid line is the least-squares fit of a second order auto-regressive model to the innovation autocorrelation function. (b) Locations of the drifting buoy SST observations used in the autocorrelation analysis.

(Hollingsworth and Lonnberg 1989). The source of this discrepancy in the background-error covariance modelling is under active investigation.

A menu-driven diagnostic package has been developed to allow end users to monitor both the quality and the performance aspects of the analysis system. Example output from the diagnostic package is shown in Fig. 7, which gives a time series of the daily temperature climate, innovation, and residual RMS and mean bias errors for the global MVOI analysis. The analysis was started from climatology on 20 June 2005 and cycled

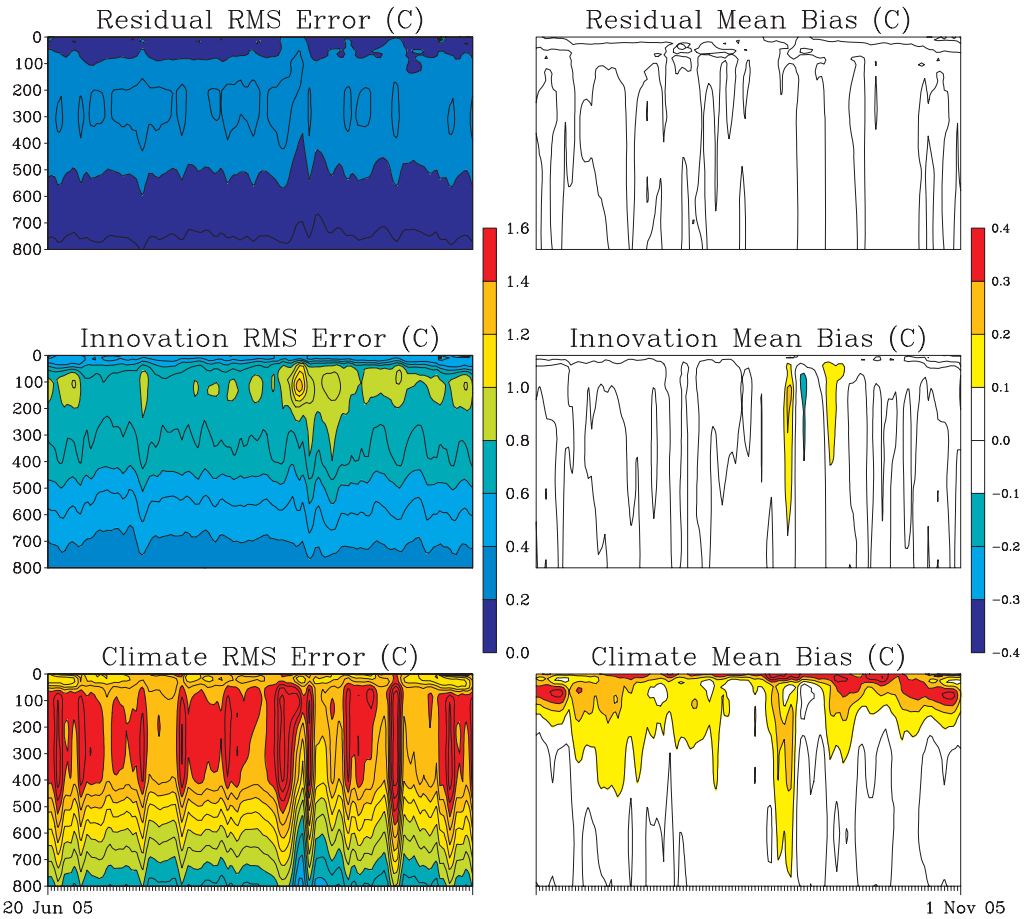

Figure 7. Daily residual, innovation and climate temperature RMS error and mean bias error statistics for global three-dimensional multivariate optimum interpolation analyses from 20 June to 1 November 2005. All sources of temperature observations are included in the error calculations. Statistics are shown for the upper 800 m of the water column. The contour interval is 0.1 degC. Each tick mark along the horizontal axes of the bottom panels represents a daily analysis update cycle.

for 135 days using a 24-hour update cycle. On average, ∼1800 *in situ* profiles are assimilated each day, along with ∼3500 MODAS synthetic profiles generated to capture daily SSHA changes measured by the altimeters using the sampling scheme described in subsection 4(c). The verification time series shows a consistent pattern of reduction in RMS error from climatology to the previous analysis (innovations). A further reduction in RMS error is also seen from the innovations to the analysis residuals. Residual and innovation mean biases are close to zero, other than during a period in early September when the transmission of satellite SST and altimeter data from NAVOCEANO was interrupted due to Hurricane Katrina. The innovation-error plots show that the analysis quickly recovered once the data transfers resumed. Residual RMS errors are a maximum at depths corresponding to high vertical gradients in the global ocean, which is consistent with the specification of the profile representation errors described previously. These results demonstrate a robust analysis, and effective use of the operational observing systems in the analysis.

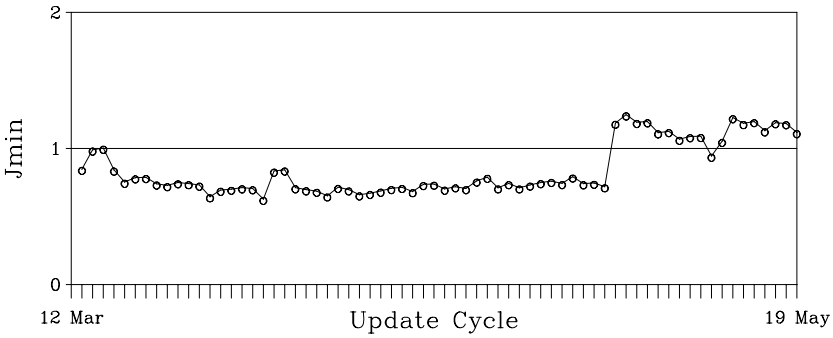

Figure 8. Time series of the $J_{\min}$ statistic (see section 5) for temperature profiles assimilated in global three-dimensional multivariate optimum interpolation analyses from 12 March to 19 May 2005. The temperature profiles assimilated include all *in situ* observations, plus synthetic temperature profiles computed from altimeter SSHA analyses using the MODAS method (see subsection 4(c)). The temperature profile representation error was adjusted on May 1.

The consistency of the specified error variances with the innovation vector is estimated by the a posteriori $J_{\min}$ diagnostic (Daley and Barker 2001). When normalized by the number of observations, the expected value of the $J_{\min}$ diagnostic is one. $J_{\min}$ values not equal to one indicate that either the background and/or observation covariances are specified incorrectly, or that erroneous observations are being assimilated. The $J_{\min}$ diagnostic is routinely computed for all observing systems and analysis variables at each update cycle. While all aspects of the analysis system affect $J_{\min}$, it is assumed in the adaptive scheme implemented here that any discrepancy of $J_{\min}$ with respect to its expected value is due to incorrect specification of the error variances. Accordingly, a simple scalar is used in the analysis to increase or decrease the observation representation and/or background-error variances. By monitoring the $J_{\min}$ diagnostic in subsequent executions of the analysis, it can be determined if the error variance scaling produces an appropriate response. For example, Fig. 8 shows a 2-month time series of daily $J_{\min}$ diagnostics computed for temperature profile observations from the global 3D MVOI analysis. Assuming that $J_{\min}$ values less than one are due to an incorrect specification of the temperature observation error variance, the temperature profile representation error was decreased on 1 May. The $J_{\min}$ diagnostic exhibited an immediate overshoot, but subsequent update cycles show the statistic approaching the expected value of one. It should be noted, however, that inferences made from the $J_{\min}$ diagnostic require very large sample sizes from many time integrations of the assimilation system.

6. Operations and future applications

As mentioned in the introduction, the NCODA multivariate analysis is running in an analysis-only, real-time operational mode at the US Navy oceanographic production centres. At FNMOC, global 9-km resolution SST and sea ice analyses are being produced as a contribution to the GODAE High Resolution SST pilot project (GHRSST-PP). The GHRSST-PP analyses are executed using a 6-hour update cycle and are available within 6 hours of real-time. In addition, a global 3D MVOI analysis executed at 18-km resolution is being produced by FNMOC. The 3D analysis assimilates the same suite of observations as the GHRSST-PP product, plus *in situ* temperature and

salinity profiles from Argo floats, shipboard CTD and expendable bathythermograph (XBT) casts, thermistor chain fixed and drifting buoys, and satellite altimeter SSHA observations assimilated via the MODAS synthetic profile approach. The global 3D MVOI analysis is executed using a 24-hour update cycle, and the analysis products are available within 9 hours of real-time. The global analysis is being used to evaluate the impact of the assimilation of Argo profiles and satellite altimeter data as a contribution to GODAE. The GHRSST-PP and the global 3D MVOI analyses are available on the US GODAE server at http://www.usgodae.org.

Two new applications of NCODA are under development. First, NCODA is being implemented as the data assimilation component of the HYCOM ocean forecast model as part of a US contribution to GODAE. This system will initially be implemented in basin-scale analysis/forecast modelling systems in the North Atlantic and North Pacific, with the ultimate aim of a fully global implementation soon thereafter. The layer structure of HYCOM presents new challenges to the assimilation system. A new analysis variable has been added that computes the correction of the model forecast isopycnal layer pressures; these are needed to match the density profile computed from the observed temperature and salinity. The correction moves model layers at their target density to the new pressure levels subject to a series of constraints that are applied after the analysis in a model initialization step (e.g. hydrostatic stability, minimum layer thickness). Evaluation of the skill of the HYCOM forecasts issued from the analyses is ongoing. The second application of NCODA is the development of an ensemble forecasting capability for application in limited-area modelling. The forecast ensembles are generated by a space–time deformation of the atmospheric forcing fields as well as a perturbation of the ocean model initial conditions using the ensemble transform technique (Bishop and Toth 1999). The ensemble of forecast perturbations is then transformed to an ensemble of analysis perturbations using the ensemble transform Kalman Filter (ETKF; Bishop *et al.* 2001). Flow-dependent covariances are derived from the ETKF and directly input into the multivariate analysis for the next control run using a hybrid error-covariance formulation (Etherton and Bishop 2004). The ensemble system will be used in an adaptive sampling, targeted observation application with ocean gliders. Ocean gliders provide up and down profiles of temperature and salinity and other variables, and the path of a glider through the water column can be controlled from the surface. The ETKF determines the way-points for the next dive of the glider and the set of glider profile observations that minimize the ocean model forecast error in a predefined verification area.

ACKNOWLEDGEMENTS

This work was funded by the Office of Naval Research 6.2 Coupled Ocean Data Assimilation project under Program Element 602435N. The Program Executive Office for C4I and Space PMW-180 provided additional funding under Program Element 603207N as part of the 6.4 project Ocean Data Assimilation for the Coupled Ocean Atmosphere Mesoscale Prediction System (COAMPS). I acknowledge the assistance of Mark Ignaszewksi at FNMOC for his help in setting up and maintaining the real-time ocean data QC and analysis system in operations. I value the efforts of the two anonymous reviewers and the associate editor who greatly helped improve the manuscript.

REFERENCES

Bishop, C. and Toth, Z. 1999 Ensemble transformation and adaptive observations. *J. Atmos. Sci.*, **56,** 1748–1765

Bishop, C. H., Etherton, B. J. and Majumdar, S. J. 2001 Adaptive sampling with the ensemble Kalman Filter. I: Theoretical aspects. *Mon. Weather Rev.*, **129,** 420–436

Chelton, D. B., DeSzoeke, R. A., Schlax, M. G., Naggar, K. E. and Siwertz, N. 1998 Geographical variability of the first baroclinic Rossby radius of deformation. *J. Phys. Oceanogr.*, **28,** 433–460

Cooper, M. and Haines, K. A. 1996 Altimetric assimilation with water property conservation. *J. Geophys. Res.*, **24,** 1059–1077

Cummings, J. A. 2006 'The NRL real-time ocean data quality control system'. NRL Technical Note, in press (preprint available from cummings@nrlmry.navy.mil)

Daley, R. 1991 *Atmospheric data analysis*. Cambridge University Press, Cambridge, UK

Daley, R. and Barker, E. 2001 NAVDAS formulation and diagnostics. *Mon. Weather Rev.*, **129,** 869–883

Etherton, B. J. and Bishop, C. H. 2004 Resilience of hybrid ensemble/3DVAR schemes to model error and ensemble covariance error. *Mon. Weather Rev.*, **132,** 1065–1080

Fofonoff, N. P. and Millard, R. C. 1983 'Algorithms for computation of fundamental properties of seawater'. Technical Paper Marine Science. UNESCO 44, Paris, France

Fox, A. D., Haines, K., de Cuevas, B. A. and Webb, D. J. 2000 Altimeter assimilation in the OCCAM global model. II: TOPEX/POSEDON and ERS-1 assimilation. *J. Mar. Syst.*, **26,** 323–347

Fox, D. N., Teague, W. J., Barron, C. N., Carnes, M. R. and Lee, C. M. 2002 The modular ocean data assimilation system. *J. Atmos. Ocean. Technol.*, **19,** 240–252

Goerss, J. and Phoebus, P. 1992 The Navy's operational atmospheric analysis. *Weather and Forecasting*, **7,** 232–249

Hollingsworth, A. and Lonnberg, P. 1986 The statistical structure of short-range forecast errors as determined from radiosonde data. I: The wind field. *Tellus*, **38A,** 111–136

1989 The verification of objective analyses: Diagnostics of analysis system performance. *Meteorol. Atmos. Phys.*, **40,** 3–27

Lorenc, A. 1981 A global three-dimensional multivariate statistical analysis system. *Mon. Weather Rev.*, **109,** 701–721

Roemmich, D., Boebel, O., Desaubies, Y., Freeland, H., Kim, K., King, B., LeTraon, P., Molinari, R., Owens, W. B., Riser, S., Send, U., Takeuchi, K. and Wijfells, S. 2001 Argo: The global array of profiling floats. Pp. 248–258 in *Observing the oceans in the 21st century*. Eds. C. J. Koblinsky and N. R. Smith. GODAE Project Office, Bureau of Meteorology Research Centre, Melbourne, Australia